Desalination and Water Treatment
www.deswater.com
doi: 10.5004/dwt.2022.28764

270 (2022) 111–126
September

Removal of Cr(VI) from aqueous solutions using polyamidoamine dendrimer-modified biochar

Jie Li, Jiangtao He, Jianhong Huang, Qun Zhao*, Yingjie Li, Senlin Tian*

Faculty of Environmental Science and Engineering, Kunming University of Science and Technology, Kunming, Yunnan 650500, China, Tel./Fax: +86-871-65920528; emails: zq441206@163.com (Q. Zhao), tiansenlin@outlook.com (S. Tian), lj478425753@163.com (J. Li), jiangtao_h@163.com (J. He), huangjianhong78@163.com (J. Huang), yjli@kmust.edu.cn (Y. Li)

Received 25 February 2022; Accepted 23 July 2022

ABSTRACT

In this study, a novel set of polyamidoamine (PAMAM) dendrimer-modified biochar adsorbents (BC-G1, BC-G2, and BC-G3) were fabricated using the "graft onto" method. The results showed that the modified biochar adsorbents, with the inclusion of amine functional groups, exhibited higher Cr(VI) removal efficiency compared with the original biochar at pH 2. The adsorption capacity of biochar adsorbents was in the following order: BC-G2 > BC-G1 > BC-G3, with maximum adsorption capacity of 120.77, 101.52, and 40.98 mg/g at 30°C, respectively. The effects of cations Cu(II), Cd(II), Mn(II), Ca(II), and K(I) or anions (Cl^-, NO_3^-, and HPO_4^{2-}) in wastewater on the adsorption of Cr(VI) were insignificant, except for SO_4^{2-}. The adsorption process of all biochar materials for removing Cr(VI) was well described using the pseudo-second-order kinetics model and Langmuir adsorption isotherm model. The Cr(VI) adsorption was primarily based on the chemical adsorption of a single molecular layer, accompanied by electrostatic interaction, reduction, and surface complexation. In addition, the adsorbents could be regenerated using a 0.2 M NaOH solution, and the adsorption capacity of the BC-G2 remains high for four adsorption–desorption cycles. Therefore, PAMAM dendrimer-based biochar adsorbent (BC-G2) can effectively remove Cr(VI) from wastewater.

Keywords: Biochar; PAMAM dendrimer; Modification; Cr(VI); Adsorption

1. Introduction

Heavy metals, such as chromium (Cr), have been a major environmental pollutant worldwide. United States Environmental Protection Agency (US EPA) categorized Cr as a priority pollutant due to its carcinogenicity, non-biodegradability, and bioaccumulation properties [1,2]. Cr is an important raw material for some industries; it is extensively used in leather tanning, electroplating, wood preservation, and cooling towers [3]. The discharge of untreated wastewater containing a high concentration of Cr can cause severe damage to plants and animals as well as humans. Generally, Cr(VI) and Cr(III) are the main forms of Cr in the natural environment, among which Cr(VI) exhibits higher toxic effects than Cr(III) [4,5]. In aqueous media, the Cr(VI) toxicity is 1,000 times higher than that of Cr(III) [6]. As a result, long-term exposure to Cr(VI) can damage the kidney and liver as well as the human circulatory system [7]. Therefore, the removal of Cr(VI) from wastewater is urgent and vital, reducing the environmental pollution.

Currently, precipitation, ion-exchange, electrodialysis, biological remediation, and adsorption methods are used to remove Cr(VI) from water [8]. Among these methods,

* Corresponding authors.

adsorption has attracted research attention owing to its cost-effectiveness, simplicity, high efficiency, and eco-friendliness advantages for toxic metal ion removal [6,9–12]. The development of inexpensive and efficient adsorbents is the key to practical and economical applications of adsorption methods [11]. Biochar is a stable heterogeneous carbonaceous material obtained through biomass pyrolysis under a limited or oxygen-free atmosphere [13,14]. Biochar is a sustainable adsorbent for removing heavy metals from wastewater due to its low-cost, availability, and eco-friendly advantages [15]. However, the low adsorption capacity and selectivity of raw biochar adsorbents hinder their potential applications in wastewater treatment [16]. Thus, recent studies have focused on surface modification of pristine biochar using various exogenous functional groups, such as carboxylic, amino, hydroxyl, and thiol, to improve their adsorption performance and increase selectivity for certain heavy metal pollutants [17,18]. In addition, studies have shown that amine-modified biochar is more effective in adsorbing anionic Cr(VI) [19]. Moreover, the performance of adsorbents is mainly influenced by the specific surface area of the materials and the density of functional groups responsible for adsorption [20]. Thus, the modification of biochar with a high density of amino functional groups would greatly improve the adsorption performance of Cr(VI).

Polyamidoamine (PAMAM) dendrimer consists of numerous cavities and peripheral amine groups with a well-defined three-dimensional hyperbranched structure. PAMAM has been used to fabricate super adsorption materials due to its unique molecular structure and the attractive binding ability for metal ions [21,22]. For instance, Lee et al. [20] used the PAMAM dendrimer to modify mesoporous silica foam or fibrous nano-silica for efficient adsorption of Gd(III). Hayati et al. [23] reported the modification of carbon nanotubes with PAMAM dendrimer to remove Cu(II) and Pb(II) from an aqueous solution with an adsorption capacity of 3,333 and 4,870 mg/g, respectively. Similarly, the PAMAM dendrimer has also been employed to prepare adsorbents for Cr(VI) removal. Zhou et al. [24] constructed the PAMAM dendrimer functionalized gel for removing Cr(VI), with a maximum adsorption capacity of 267.4 mg/g. Liu et al. [25] reported the removal of Cr(VI) from an aqueous solution with graphene oxide/polyamidoamine dendrimer composites. Therefore, modification of biochar with PAMAM dendrimer would enhance the adsorption capacity of biochar adsorbent toward Cr(VI). Meanwhile, surface amino groups of modified biochar adsorbents are actively working to make a stable complex with anionic Cr(VI) at a specific pH region. Thus, the modified biochar adsorbents can effectively adsorb Cr(VI) with high adsorption capacity and selectivity.

Specifically, PAMAM dendrimer-based adsorbents can be fabricated via "graft from" or "graft onto" methods. Graft onto methods have an advantage in direct grafting of a certain PAMAM dendrimer with control geometry regularity of the substrates through coupling attachment [22]. Therefore, in this study, PAMAM dendrimer was used to modify a novel set of biochar sorbents via a "graft onto" method to enhance Cr(VI) removal in an aqueous solution. Moreover, different generations of PAMAM dendrimer-modified biochar adsorbents were prepared to investigate the effect of the density of functional groups on the adsorption capacity. The synthesized sorbents were characterized using Fourier-transform infrared spectroscopy (FTIR), X-ray photoelectron spectroscopy (XPS), scanning electron microscope (SEM), and N_2 adsorption/desorption as well as thermogravimetric analysis (TGA). The effects of different parameters, such as solution pH, contact time, adsorbent dosage, initial concentration of Cr(VI), temperature, and coexisting ions on the adsorption performance of the modified biochar adsorbents toward Cr(VI) were investigated. In addition, adsorption kinetics, adsorption isotherms, and adsorption mechanisms of the modified biochar adsorbents were studied. Furthermore, the regeneration and repeated cycles of sorbents were evaluated for effectiveness in practical application.

2. Materials and methods

2.1. Materials

Rice straw biomass, collected from farmlands in Kunming, Yunnan Province, China, was used as the feedstock for preparing biochar. Ethylenediamine (EDA), methylacrylate (MA), 1-ethyl-3-(3-dimethyl-aminopropyl) carbodiimide hydrochloride (EDC·HCl), N-hydroxyl succinimide (NHS), and 1,5-diphenylcarbazide were purchased from Aladdin industrial corporation (Shanghai, China). Other reagents used in this study included $K_2Cr_2O_7$, HNO_3, HCl, NaOH, $CuCl_2{\cdot}2H_2O$, $CdCl_2{\cdot}2.5H_2O$, $MnCl_2{\cdot}4H_2O$, $CaCl_2$, KCl, NaCl, $NaNO_3$, Na_2SO_4, Na_2HPO_4, ethanol, and toluene, all of which were analytical grade, and they were purchased from Shanghai Macklin Biochemical Co., Ltd., China. Deionized (DI) water (18.2 MΩ) was used for all experiments. The first-generation PAMAM dendrimer (G1), second-generation PAMAM dendrimer (G2), and third-generation PAMAM dendrimer (G3) were synthesized according to the procedures described in the previously reported work [26].

2.2. Characterization

The functional groups of biochar samples were identified using FTIR (VERTEX 70, Bruker, Germany) at the wavelength ranging from 4,000 to 600 cm^{-1}. The state of the adsorbent elements before and after adsorption was analyzed using XPS (K-Alpha 1063, Thermo Fisher Scientific, USA). The surface morphology of the adsorption materials was investigated using SEM (JSM-7610 F, Japan Electronics, Japan). The N_2 adsorption/desorption isotherm was measured at liquid nitrogen temperature (77 K) using a volumetric adsorption analyzer (Tristar-3000, Micromeritic, USA). The specific surface area was calculated using Brunauer–Emmett–Teller (BET) method. The pore-size distributions of micropores and mesopores of samples were examined using the Horvath–Kawazo and Barrett–Joyner–Halenda methods, respectively. The point zero charges (pH_{PZC}) were measured using the method described by Zhang et al. [27]. The TGA curves were recorded using Jupiter thermal analyzer (Netzsch, STA409PC, Germany) at temperatures ranging from 25°C to 800°C under N_2 at a heating rate of 20°C/min.

2.3. Preparation of carboxylated biochar

Rice straw was used as feedstock to produce biochar in an oxygen-limited condition at 400°C and a heating rate of 10°C/min in a muffle furnace for 3 h. The solid residue was collected, ground, sieved (to pass through 100-mesh, 0.15 mm), and then repeatedly washed with DI water until its pH was constant. The washed biochar was dried overnight at 70°C, and it was named pristine biochar (BC). Then, the obtained biochar was modified with nitric acid to prepare carboxylated biochar. Pristine biochar (20.0 g) was added to a solution of DI water (100 mL) and HNO_3 (100 mL), and the mixture was kept at 60°C for 12 h. Finally, the solid prodcut was filtered and then rinsed with DI water and ethanol. The product was dried at 70°C for 24 h and then named carboxylated biochar (BC-COOH).

2.4. Preparation of PAMAM dendrimer modified biochar

The PAMAM dendrimer-modified biochar was synthesized via the "graft onto" method by forming an amide bond between the carboxy of BC-COOH and the amine of PAMAM dendrimer end functional groups [28]. DI water (60 mL) and BC-COOH (6 g) were added to a 500 mL three-stoppered flask; then, EDC·HCl (6 g) and NHS (4 g) were added to the mixture. After shaking the obtained mixture for 1 h at room temperature, a solution of G2 (12 g) was dissolved in methanol (120 mL), introduced into the mixture, and then reacted at 80°C for 24 h. The solid product was filtered and washed with DI water and ethanol. Then, the solid product was dried and named G2 modified biochar (BC-G2). The preparation procedures are shown in Fig. 1. G1 modified biochar (BC-G1) and G3 modified biochar (BC-G3) were obtained using G1 and G3 as the amination reagent, respectively.

2.5. Static adsorption studies

A stock solution of Cr(VI) (1000 mg/mL) was obtained by dissolving $K_2Cr_2O_7$ in DI water, and the obtained solution was diluted to the desired concentration. The static adsorption experiments were performed by mixing different qualities of adsorbents with 10 mL of Cr(VI) aqueous solution. Then, the mixture was agitated at 150 rpm in a thermostatic shaking incubator to reach an equilibrium. The influence of different parameters, such as solution pH (2–8), contact time (0.5–36 h), initial Cr(VI) concentration (25–200 mg/L), adsorbent dosage (0.3–1.2 g/L), temperature (20°C–50°C), and coexisting ions (Cu(II), Cd(II), Mn(II), Ca(II), K(I), Cl^-, NO_3^-, HPO_4^{2-}, and SO_4^{2-}), on Cr(VI) removal was investigated. The pH of the simulated wastewater was adjusted with 1 M HCl and 1 M NaOH solution. After adsorption, the solid and liquid phases were separated through a 0.45-μm filter. The residual concentration of Cr(VI) was detected with a UV–vis spectrophotometer at the wavelength of 540 nm using the 1,5-diphenylcarbazide colorimetric method [29]. The adsorption capacity (q_e) was calculated using the following equation:

$$q_e = \frac{(C_0 - C_e) \times V}{m} \tag{1}$$

where C_0 (mg/L) and C_e (mg/L) are the initial and final Cr(VI) concentrations, respectively, V (L) is the volume of solution, and m (g) is the mass of the biochar sample.

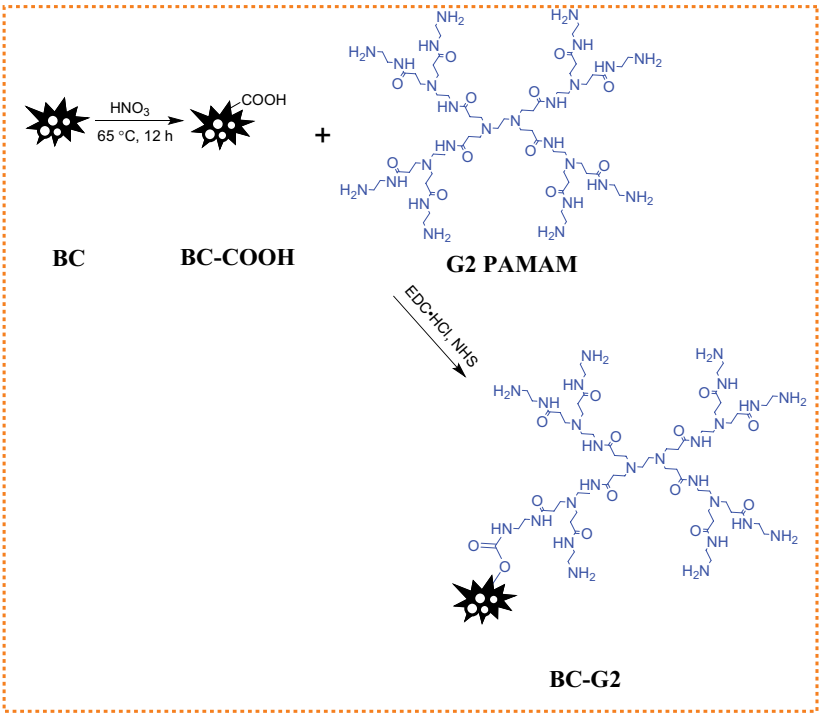

Fig. 1. The preparation procedures of BC-G2.

For adsorption kinetics, 5 mg of modified biochar adsorbents was added to 10 mL of Cr(VI) solution at 50 mg/L with different contact times ranging from 0.5 to 36 h. The pH value of the Cr(VI) solution was adjusted to 2. The obtained experimental data were fitted with three recognized kinetic models: pseudo-first-order [Eq. (2)], pseudo-second-order [Eq. (3)], and intraparticle diffusion models [Eq. (4)], as follows:

$$\ln\left(q_e - q_t\right) = \ln q_e + k_1 t \tag{2}$$

$$\frac{t}{q_t} = \frac{1}{k_2 q_e^2} + \frac{1}{q_e} t \tag{3}$$

$$q_t = k_{ip} t^{\frac{1}{2}} + C \tag{4}$$

where q_e and q_t denote the adsorption capacity at equilibrium and time t (mg/g), respectively; k_1 (1/h), k_2 (g/mg/h), and k_{ip} (mg/g/h$^{1/2}$) represent the rate constants of the pseudo-first-order, pseudo-second-order kinetic, and intraparticle diffusion models, respectively; and C is the intercept of intraparticle diffusion model related to the thickness of the boundary layer.

To study the adsorption isotherm, 5 mg of modified biochar samples was mixed with Cr(VI) solution of different concentrations (25, 50, 75, 100, 125, 150, 175, and 200 mg/L) at 30°C. After shaking the solution for 24 h, the residual concentration of Cr(VI) was determined as mentioned above. The Langmuir [Eq. (5)] and Freundlich [Eq. (6)] models (well-known and widely used models) were used to fit the adsorption isotherm data.

$$\frac{C_e}{q_e} = \frac{1}{q_{max} K_L} + \frac{C_e}{q_{max}} \tag{5}$$

$$\ln q_e = \ln K_F + \frac{1}{n} \ln C_e \tag{6}$$

$$R_L = \frac{1}{1 + K_L C_0} \tag{7}$$

where q_e and q_{max} are the equilibrium and maximum adsorption capacity (mg/g), respectively. C_e (mg/L) is the equilibrium concentration of Cr(VI), C_0 (mg/L) is the original Cr(VI) concentration, R_L (Eq. 7) is the separation factor constant for estimating the applicability of adsorbents toward Cr(VI), K_L (L/mg) and K_F (mg^{1-n} L^n/g) are the constants of Langmuir and Freundlich models, respectively, and n is the adsorption intensity index.

The Langmuir model considers a monolayer homogenous chemisorption having finite active sites without interaction between the adsorbents [30], while the Freundlich isotherm assumes multilayer uptake of adsorbates on the active sites with heterogeneous energetic distribution [31].

The thermodynamic parameters $\Delta G°$, $\Delta H°$, and $\Delta S°$ were used to study the thermodynamics of Cr(VI) adsorption using modified biochar samples according to the following equations:

$$K_c = \frac{q_e}{C_e} \tag{8}$$

$$\ln K_c = -\frac{\Delta H°}{RT} + \frac{\Delta S°}{R} \tag{9}$$

$$\Delta G° = \Delta H° - T\Delta S° \tag{10}$$

where q_e (mg/g) and C_e (mg/L) are the equilibrium adsorption capacity and concentration of Cr(VI), respectively; T is the temperature; R (8.314 J/mol/K) is the general gas constant; and $\Delta S°$, $\Delta H°$, and $\Delta G°$ are the entropy, enthalpy change, and change of Gibbs free energy, respectively.

Adsorption–desorption experiment was used to study the stability and reusability of biochar adsorbents. After adsorption, the biochar samples were washed with 0.2 M of NaOH, and the suspension was shaken for 12 h during the desorption. The adsorbents were filtered, washed with deionized water, dried, and then used in the next cycle.

3. Results and discussion

3.1. Characterization

The FTIR spectra of the biochar samples are shown in Fig. 2a. The peaks located at 1,597 and 1,070 cm^{-1} in the BC spectrum were assigned to the stretching of aromatic C=C and C–O–C groups, respectively [32]. The peaks of all the biochar samples at 798 cm^{-1} were attributed to the stretching of aromatic carbon [33]. After treating BC with HNO_3, a new peak at 1,710 cm^{-1} corresponding to the carbonyl groups (–C=O) was observed [34], confirming the oxidation of biochar. Moreover, peaks at 1,534 and 1,336 cm^{-1} represented NO_2 ν_{asym} and NO_2 ν_{sym}, respectively, which indicated that some nitro groups were incorporated into the BC-COOH [35]. In the spectra of BC-G1, BC-G2, and BC-G3, new characteristic peaks at 1,642 and 1,543 cm^{-1} were well explained with the amide group (CO–NH) of type I and type II, respectively, which indicated that PAMAM dendrimer had been successfully grafted onto the BC surface through chemical bonding [22,23,36]. When compared to BC-G1 and BC-G2 spectra, BC-G3 spectra exhibited a clear peak at 1,710 cm^{-1}, suggesting that certain amounts of carboxylic groups remain on the biochar after G3 functionalization. This phenomenon may be attributed to the strong steric hindrance, leading to a lower percentage of G3 grafted on the BC surface [37].

The variations in the elemental composition of the biochar sample surfaces were investigated using XPS (Fig. 2b), and the related data are presented in Table 1. As shown in Fig. 2b, all the biochar samples contained similar elemental compositions, such as carbon (C), nitrogen (N), and oxygen (O), with the characteristic peaks at 284.9 (C 1s), 399.9 (N 1s), and 531.9 eV (O 1s), respectively. Although there is no considerable difference in the elemental peak of biochar samples, an increase in the intensity of N 1s peaks in BC-G1, BC-G2, and BC-G3 was observed when compared

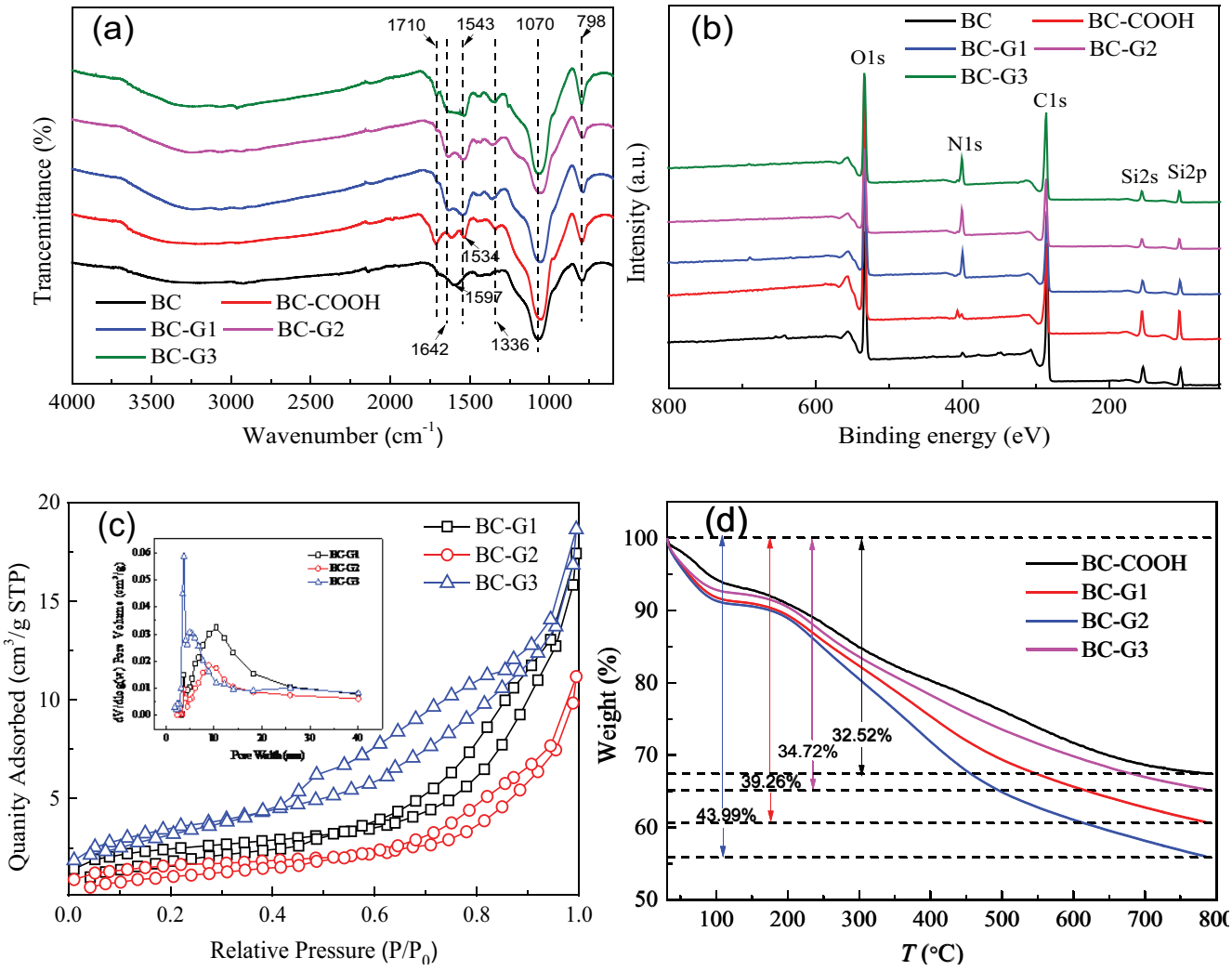

Fig. 2. FTIR spectra (a) and XPS wide-scan spectra (b) of biochar samples, N_2 adsorption–desorption isotherms (c) and pore-size distribution (inset) of BC-G1, BC-G2 and BC-G3, TGA results of the prepared BC-COOH, BC-G1, BC-G2 and BC-G3 (d).

Table 1
Elemental composition of BC, BC-COOH, BC-G1, BC-G2 and BC-G3 determined by XPS analysis

Sorbents	Atom percent (%)		
	C (%)	N (%)	O (%)
BC	57.34	1.52	24.61
BC-COOH	48.87	3.69	46.78
BC-G1	48.63	9.19	26.26
BC-G2	50.45	11.24	25.39
BC-G3	59.68	10.42	29.57

to that of BC and BC-COOH surface. Moreover, Si 2s and Si 2p peaks were observed, which may be derived from the silicon minerals of rice straw biomass [38]. Table 1 shows that there was an increase in the content of O of biochar after oxidation, which was attributed to the increase in oxygenated functionalities. Additionally, an increase in the content of N was observed, and it was thought to be associated with the incorporation of nitro groups on the surface of BC-COOH, which is in agreement with the FTIR results discussed earlier. Meanwhile, the N content of BC-G1 (9.19%), BC-G2 (11.24%), and BC-G3 (10.42%) was monitored.

The N_2 adsorption/desorption isotherm and the pore-size distribution of the synthesized biochar sorbents are shown in Fig. 2c, and the results are listed in Table 2. As shown in Fig. 2c, the isotherm curve of all the biochar samples was identified as a typical type IV curve with an H3 hysteresis loop, indicating the existence of mesopores on the adsorbent [39–41]. As shown in Table 2, the BET surface areas of BC-G1, BC-G2, and BC-G3 were 8.678, 5.665, and 12.709 m^2/g, respectively, and the pore volumes for BC-G1, BC-G2, and BC-G3 were 0.0269, 0.0171, and 0.0289 cm^3/g, respectively. As the grafted generation of PAMAM dendrimer increased, the biochar materials showed a gradual decrease in BET surface area and pore volume, which can be attributed to the increase in the molecular volume of high-generation dendrimer occupying the pores and the decrease in the surface area and pore volume [22,42].

Table 2
Pore structure parameters of BC-G1, BC-G2 and BC-G3

Sorbents	Surface area (m^2/g)	Pore diameter (nm)	Pore volume (cm^3/g)
BC-G1	8.678	11.450	0.0269
BC-G2	5.665	12.146	0.0171
BC-G3	12.709	7.644	0.0289

Regarding BC-G3, the strong steric hindrance led to a lower percentage of G3 grafted on the biochar; thus, a modified biochar adsorbent with large BET surface areas and pore volumes was obtained. Despite the small pore volume and BET surface area in all the modified biochar adsorbents, the samples still efficiently adsorb Cr(VI) owing to the abundant active sites of functional groups, as revealed in FTIR and XPS analyses.

The thermal stabilities of BC-COOH, BC-G1, BC-G2, and BC-G3 are shown in Fig. 2d. The weight loss of all the biochar sorbents can be divided into two distinct stages. In the first stage, the weight loss at temperatures below 200°C was attributed to evaporation of the absorbed water and pyrolysis of the oxygen-containing groups [43]. The second stage of weight loss was observed at temperatures between 200°C and 800°C, which was attributed to the thermal decomposition of the dendrimer layer and the stable functional groups [44]. The final weight loss of BC-G1, BC-G2, and BC-G3 was 39.26%, 43.99%, and 34.72%, respectively, corresponding to ca. 6.75, 11.47, and 2.17 wt.% of G1, G2, and G3, respectively, grafted on the biochar [20].

Fig. 3 depicts the surface morphology microstructure of the biochar samples, observed through SEM. Fig. 3a shows the uniform distribution of a neat surface and the honeycomb structure on the BC surface. The porous surface structure of BC was even and regular. When the biomass was pyrolyzed, a volatile gaseous substance generated by some of the organic compounds of biomass was released, resulting in the formation of morphological microstructures [6,45]. Compared with Fig. 3a and b shows some collapsed pores of BC-COOH. This was related to the addition of HNO_3. As shown in Fig. 3c–e, the honeycomb fracture surface was maintained after the bonding of PAMAM dendrimer onto biochar, which indicated that the surface morphology of biochar was hardly influenced by the functional modification [46].

3.2. Effect of different parameters on Cr(VI) adsorption

3.2.1. Effect of solution pH on Cr(VI) adsorption capacity

Studies have shown that the pH value of aqueous solutions affects the existing species of metals and the charge properties of the adsorbent [47]. The main forms of Cr(VI) were $HCrO_4^-$ and $Cr_2O_7^{2-}$ within the pH range of 1–6, whereas CrO_4^{2-} was predominant at pH = 7–10 [48]. Fig. 4a shows the effect of solution pH on the Cr(VI) adsorption capacity of the three different modified biochar samples. The adsorption capacity of all the adsorbents for removing Cr(VI) significantly decreased as the solution pH increased from 2 to 8. This phenomenon has been observed in other studies [24,48,49], and it could be attributed to the electrostatic attraction between the negatively charged Cr(VI) anions and positively charged biochar surface at a lower pH [49]. In addition, the point of zero charges (pH_{PZC}) of BC-G1, BC-G2, and BC-G3 (Fig. 4b) was 6.39, 6.55, and 4.74, respectively. When the pH of the solution was lower than the pH_{PZC}, the functional groups on the biochar surface would be protonated, which is beneficial for the adsorption of Cr(VI) anions. The adsorption capacity decreased with increasing pH, which may be a result of a few positively charged surfaces associated with weak electrostatic attraction toward Cr(VI) ions [24]. These results showed that the adsorption behavior of PAMAM dendrimer-modified biochar adsorbents was significantly affected by the pH of the solution, and the highest Cr(VI) adsorption capacity was achieved at pH = 2. Thus, subsequent experiments were conducted at a pH of 2 to obtain the optimal adsorption performance.

3.2.2. Effect of PAMAM generations on Cr(VI) adsorption capacity

Different biochar adsorbents were applied to remove Cr(VI). As shown in Fig. 5a, the adsorption capacity of Cr(VI) showed a significant increase after the modification of the biochar with the PAMAM dendrimer. The adsorption capacities of BC-G1, BC-G2, and BC-G3 for Cr(VI) removal were 69.5, 75.8, and 31.7 mg/g, respectively, at a pH of 2, which were much higher than that of BC (25.6 mg/g) and BC-COOH (12.1 mg/g). The adsorption capacities of these functionalized sorbents followed the sequence of BC-G2 > BC-G1 > BC-G3, which is similar to the result reported by Qin et al. [37] in the study of Hg(II) uptake properties of polyacrylamide/ATP (PAMAM-ATP). This phenomenon could be attributed to the generation number and the steric hindrance of the PAMAM dendrimer. When the generation number of PAMAM dendrimers increases, the number of G2 functional groups grafted onto biochar increase the adsorption capacity of BC-G2 compared to BC-G1. However, the strong steric hindrance of G3 led to a lower percentage of functional groups on the basal plane of BC-G3, thus decreasing the adsorption capacity of BC-G3 [37].

3.2.3. Effect of contact time and adsorbent dosage on Cr(VI) adsorption capacity

The effect of contact time on Cr(VI) adsorption capacity is illustrated in Fig. 5b. The amount of adsorbed Cr(VI) increased rapidly in the first half-hour owing to abundant active sites of absorbents, with the higher Cr(VI) concentration acting as the driving force. Subsequently, the adsorption capacity of biochar adsorbents gradually decreased

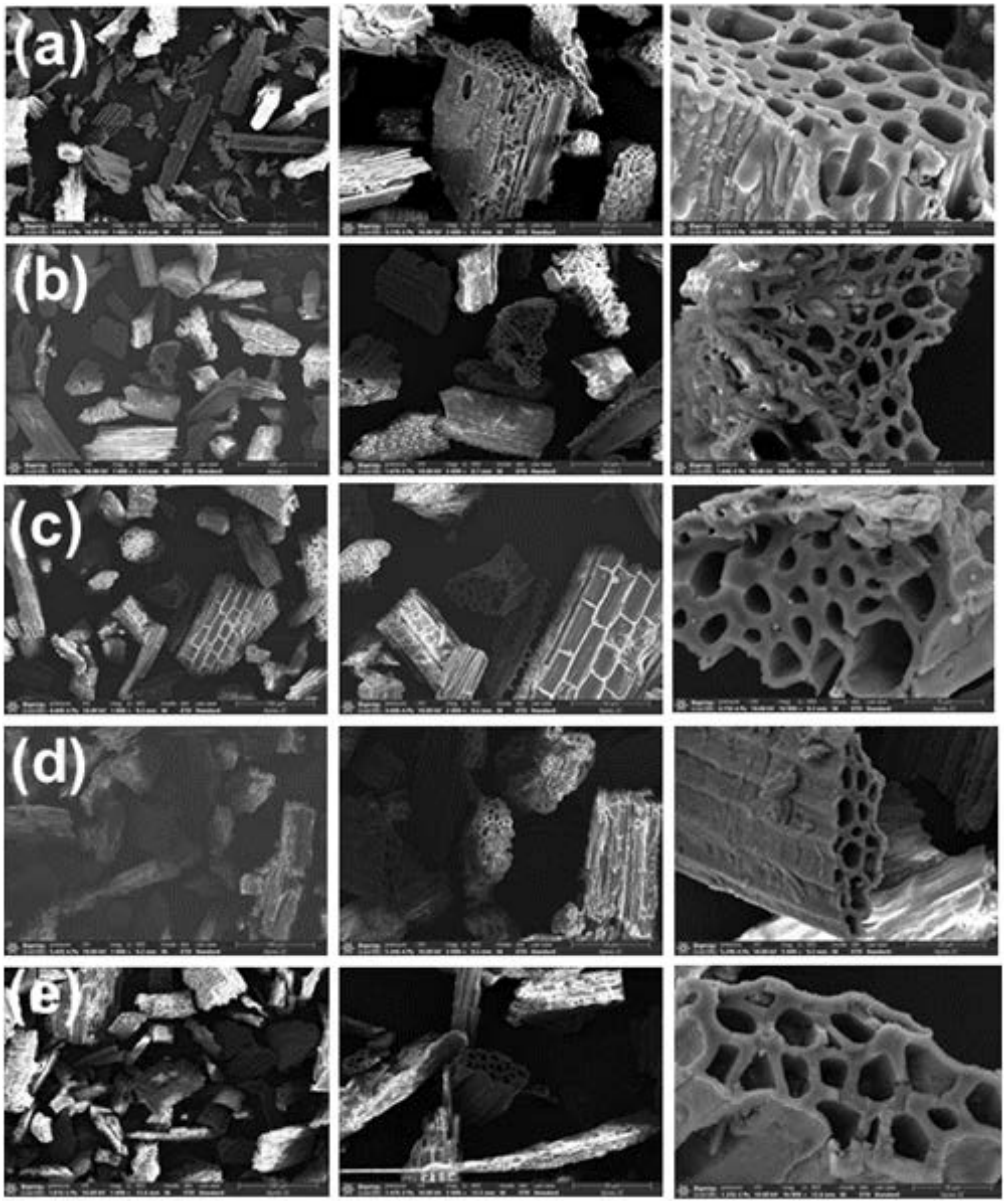

Fig. 3. SEM images of BC (a), BC-COOH (b), BC-G1 (c), BC-G2 (d) and BC-G3 (e).

and then reached an equilibrium with increasing contact time. This phenomenon may be attributed to the decreasing active sites and repulsive forces between absorbed and unabsorbed Cr(VI) [6]. The effect of biochar adsorbent dosages on Cr(VI) uptake is illustrated in Fig. 5c. The amounts of Cr(VI) adsorbed decreased with an increase in adsorbent dosage. The result might be attributed to the availability of active sites at lower absorbent doses and aggregation of adsorption particles at higher adsorbent doses [50]. Similar results have been previously reported in other studies [11,50].

3.2.4. Effect of initial Cr(VI) concentration and temperature on Cr(VI) adsorption capacity

The adsorption capacity of biochar adsorbents for Cr(VI) increased with an increase in the initial concentration of Cr(VI) (Fig. 5d), which at a higher concentration creates a larger concentration gradient between the liquid phase and the biochar adsorbent surface [11]. The influence of adsorption temperature on the adsorption capacity of biochar samples for removing Cr(VI) is shown in Fig. 5e. The adsorption capacity of all the adsorbents increased as the temperature rose from 20°C to 50°C, meaning that the removal of Cr(VI) using the modified biochar adsorbent was an endothermic process [48].

3.2.5. Effect of coexisting cations on Cr(VI) adsorption capacity

The actual wastewater containing other soluble ions may affect the adsorption capacity of Cr(VI) to some extent. Thus, the influence of coexisting cations on Cr(VI)

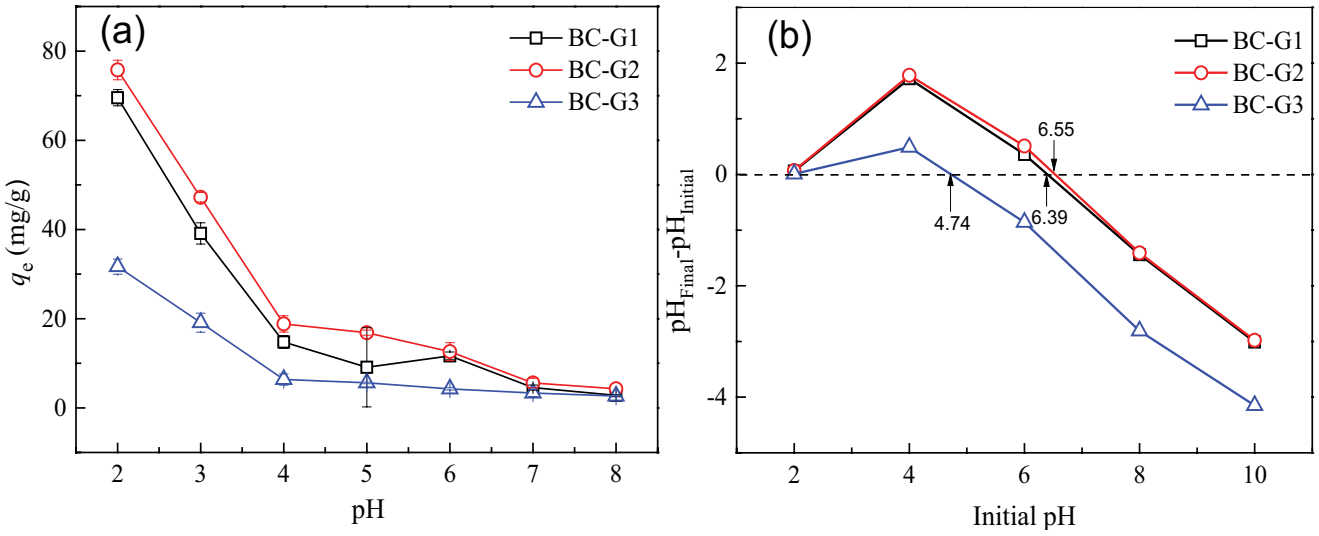

Fig. 4. Effect of solution pH on the adsorption of Cr(VI) by BC-G1, BC-G2 and BC-G3 (a) and the point of zero charge (pH_{PZC}) of three biochar sorbents (b) (temperature: 30°C, contact time: 24 h, dosage: 0.5 g/L, initial Cr(VI) concentration: 50 mg/L).

adsorption of BC-G1, BC-G2, and BC-G3 were investigated. The concentrations of Cr(VI) and each coexisting ion were maintained at 50 mg/L. As shown in Fig. 6a, the coexisting cations Cu(II), Cd(II), Mn(II), Ca(II), and K(I) had limited influence on Cr(VI) removal. The impact of coexisting anions Cl^-, NO_3^-, and HPO_4^{2-} on the adsorption capacities of three biochar adsorbents for removing Cr(VI) was relatively low. However, the existence of SO_4^{2-} significantly reduced the adsorption capacities of adsorbents (Fig. 6b). This phenomenon indicated that SO_4^{2-} could compete with Cr(VI) anions on the adsorbents to a certain extent owing to the similarity in SO_4^{2-} and $Cr_2O_7^{2-}$ molecular structures and their negative charges, leading to the decrease in the removal efficiency of Cr(VI) [51]. This phenomenon is consistent with previously reported works [7,51].

3.3. Adsorption modeling

3.3.1. Adsorption kinetics

The pseudo-first-order model and the pseudo-second-order model were used to investigate the adsorption process of materials. The fitted plots of these models for Cr(VI) sorption are shown in Fig. 7a and b. The fitted parameters and correlation coefficients are listed in Table 3. The correlation coefficient R^2 of all the biochar adsorbents for the pseudo-second-order model is higher than that of the pseudo-first-order model, which indicates that the pseudo-second-order model is adequate to depict the adsorption kinetics of Cr(VI). Meanwhile, the adsorption capacities calculated by the pseudo-second-order model ($q_{e,cal}$) are consistent with the experimental equilibrium ($q_{e,exp}$). The results suggested that the adsorption of Cr(VI) using the PAMAM dendrimer-modified biochar was based on chemical adsorption, meaning the electron transfer, exchange or sharing was generated and chemical bond was formed in the adsorption process [44]. Moreover, the fitting results of the intraparticle diffusion model are shown in Fig. 7c. The fitted line of all the biochar samples of q_t and $t^{1/2}$ does not pass through the origin, revealing that intraparticle diffusion is not the only rate-controlling step in the entire adsorption process [11].

3.3.2. Adsorption isotherm

In order to investigate the interaction behaviors between adsorbate and adsorbent, the sorption isotherms of Cr(VI) onto the biochar materials were simulated using the Langmuir and Freundlich models. The fitting results are shown in Fig. 7d and e. The corresponding correlation coefficients and constants are listed in Table 4. The results showed that the Langmuir isotherms (R^2 = 0.9775–0.9971) had a better line-fitting effect than the Freundlich isotherms (R^2 = 0.6133–0.9273), suggesting that the Langmuir

Table 3
Parameters and determination coefficients of the kinetic models for the uptake of Cr(VI) onto BC-G1, BC-G2 and BC-G3

Sorbents	$q_{e,exp}$ (mg/g)	Pseudo-first-order model			Pseudo-second-order model			Intraparticle diffusion model		
		$q_{e,cal}$ (mg/g)	k_1 (1/h)	R^2	$q_{e,cal}$ (mg/g)	k_2 (g/mg/h)	R^2	k_{ip}	C	R^2
BC-G1	68.05	20.23	0.1292	0.9782	70.87	0.0158	0.9985	4.3206	47.0306	0.9227
BC-G2	77.92	21.02	0.1436	0.9123	79.74	0.0207	0.9988	4.1857	57.1967	0.9008
BC-G3	32.56	16.30	0.1129	0.9705	36.18	0.0126	0.9905	3.6416	14.865	0.9696

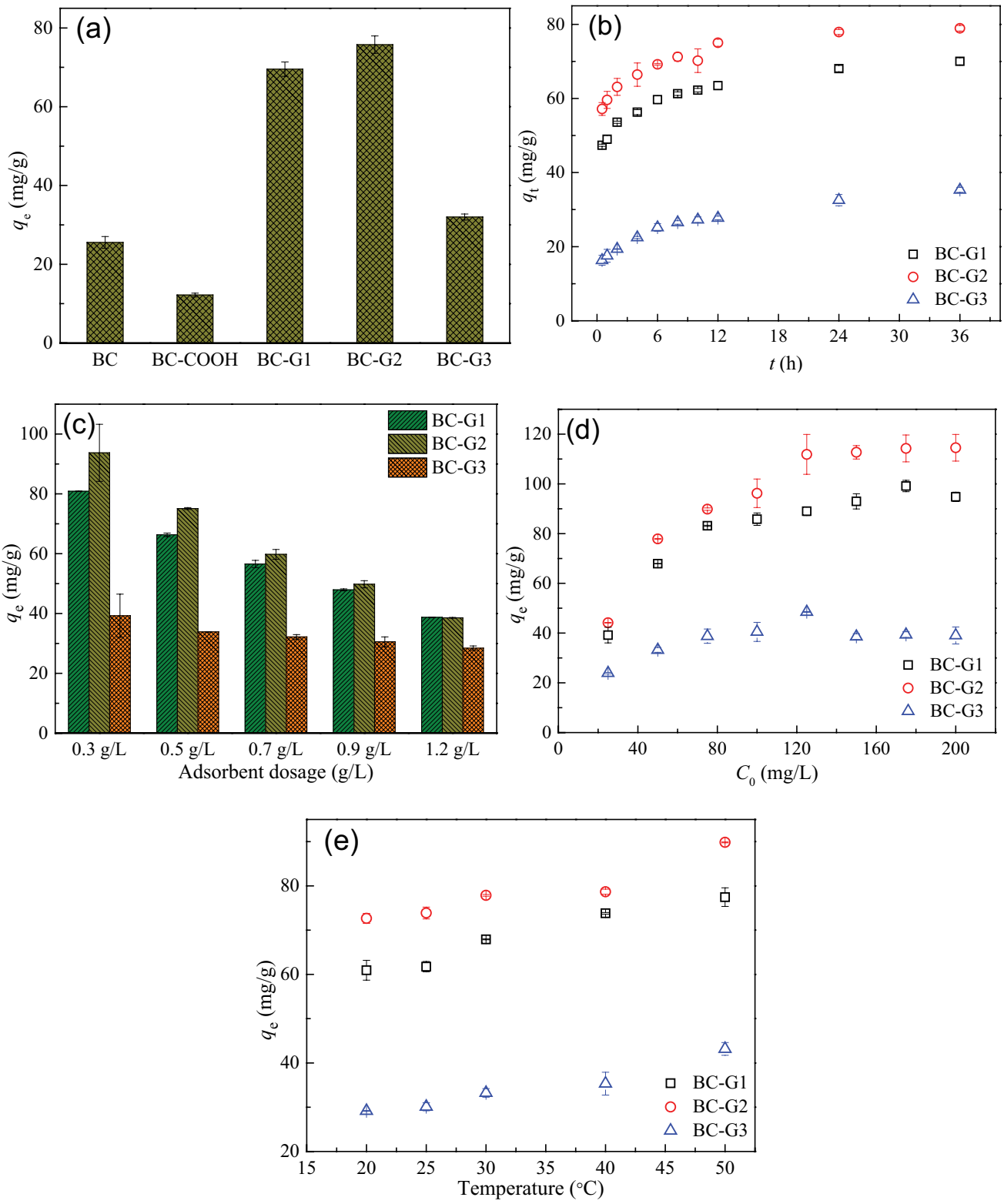

Fig. 5. Effect of BC-G1, BC-G2 and BC-G3 on adsorption of Cr(VI): PAMAM generations (a), contact time (b), adsorbent dosage (c), initial Cr(VI) concentration (d) and temperature (e) [(a) pH = 2, temperature: 30°C, contact time: 24 h, dosage: 0.5 g/L, initial Cr(VI) concentration: 50 mg/L, (b) pH = 2, temperature: 30°C, dosage: 0.5 g/L, initial Cr(VI) concentration: 50 mg/L, (c) pH = 2, temperature: 30°C, contact time: 24 h, initial Cr(VI) concentration: 50 mg/L, (d) pH = 2, temperature: 30°C, contact time: 24 h, dosage: 0.5 g/L, (e) pH = 2, contact time: 24 h, dosage: 0.5 g/L, initial Cr(VI) concentration: 50 mg/L)].

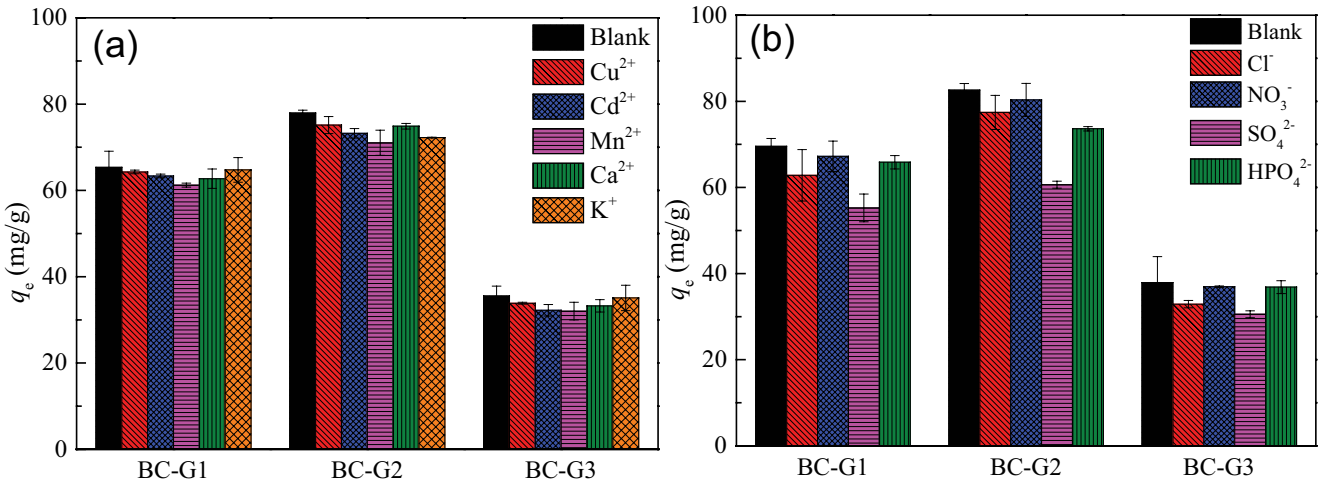

Fig. 6. Effect of coexisting cations (a) and anions (b) on the adsorption of Cr(VI) of BC-G1, BC-G2 and BC-G3 (pH = 2, temperature: 30°C, contact time: 24 h, dosage: 0.5 g/L, initial Cr(VI) concentration: 50 mg/L).

Table 4
Parameters and determination coefficients of the isotherm models for Cr(VI) adsorption on BC-G1, BC-G2 and BC-G3

Sorbents	$q_{e,exp}$ (mg/g)	Langmuir				Freundlich		
		R_L	$q_{max,cal}$ (mg/g)	K_L (1/h)	R^2	K_F	n	R^2
BC-G1	99.14	0.0415–0.2574	101.52	0.1154	0.9971	30.0445	4.0098	0.8685
BC-G2	114.52	0.0369–0.2347	120.77	0.1304	0.9964	38.4039	4.2205	0.9273
BC-G3	39.38	0.0190–0.1267	40.98	0.2757	0.9775	16.5249	5.2857	0.6133

model is more suitable for describing the sorption behavior as monolayer coverage on the adsorbents [12,30,52,53]. The adsorption capacities ($q_{max,cal}$) values of BC-G1, BC-G2, and BC-G3 calculated by Langmuir model for Cr(VI) are 101.52, 120.77, and 40.98 mg/g, respectively. Specifically, the value of R_L could reveal the adsorption tendency: irreversible (R_L = 0), favorable (0 < R_L < 1), linear (R_L = 1), or unfavorable (R_L > 1) [48]. Herein, the values of R_L in all concentrations were between 0 and 1; thus, the adsorption process was considered favorable.

3.3.3. adsorption thermodynamics

According to Fig. 5e, Eqs. (8)–(10) were used to calculate the thermodynamic parameters of Cr(VI) adsorption by modified biochar samples. The linear fit of lnK_c vs. T^{-1} is shown in Fig. 7f, and the corresponding parameters are listed in Table 5. The negative values of $\Delta G°$ reveal the spontaneous nature and feasibility of the Cr(VI) adsorption process onto the biochar adsorbents. Moreover, the $\Delta G°$ became more negative at higher temperatures, which indicated that the increase in temperature favored the adsorption of Cr(VI) ions. However, the $\Delta G°$ values of BC-G3 at 20°C, 25°C, and 30°C were positive, representing non-spontaneous behavior, which may be attributed to the special cavity and hindrance of the sorbent formed in the preparation process by grafting G3 on biochar [37]. The positive values of $\Delta H°$ confirmed that the adsorption was an endothermic process. The positive values of $\Delta S°$ showed that the disorderliness of the solid/liquid interface increased during the adsorption process [48]. These results indicated that higher temperatures would benefit the process to overcome the reaction resistance and accelerate the adsorption process.

3.4. Adsorption mechanism analysis

The XPS analyses were used to clarify the adsorption mechanism, taking BC-G2 as an example. The results of XPS full survey spectra are shown in Fig. 8a. A new peak resulting from the photoelectron peak of Cr 2p appeared after the adsorption, suggesting that Cr(VI) was absorbed on the biochar surface, which was further confirmed through the high-resolution Cr 2p spectra (Fig. 8b). The peaks at 578.9 and 587.9 eV corresponded to the Cr $2p_{3/2}$ and Cr $2p_{1/2}$ of Cr(VI), respectively. Meanwhile, the peaks at 576.9 and 586.3 eV were assigned to the Cr $2p_{3/2}$ and Cr $2p_{1/2}$ of Cr(III), respectively. The results indicated that both Cr(III) and Cr(VI) were present on the surface of BC-G2, and the part of Cr(VI) adsorbed on the surface was reduced to Cr(III) [54]. The relatively high fraction (67.68%) of Cr(III) indicated a significant contribution of Cr(VI) reduction rather than direct Cr(VI) adsorption.

The high-resolution C 1s spectra of BC-G2 before and after the adsorption of Cr(VI) are shown in Fig. 8c and d, respectively. Before adsorption, the binding energy peaks at

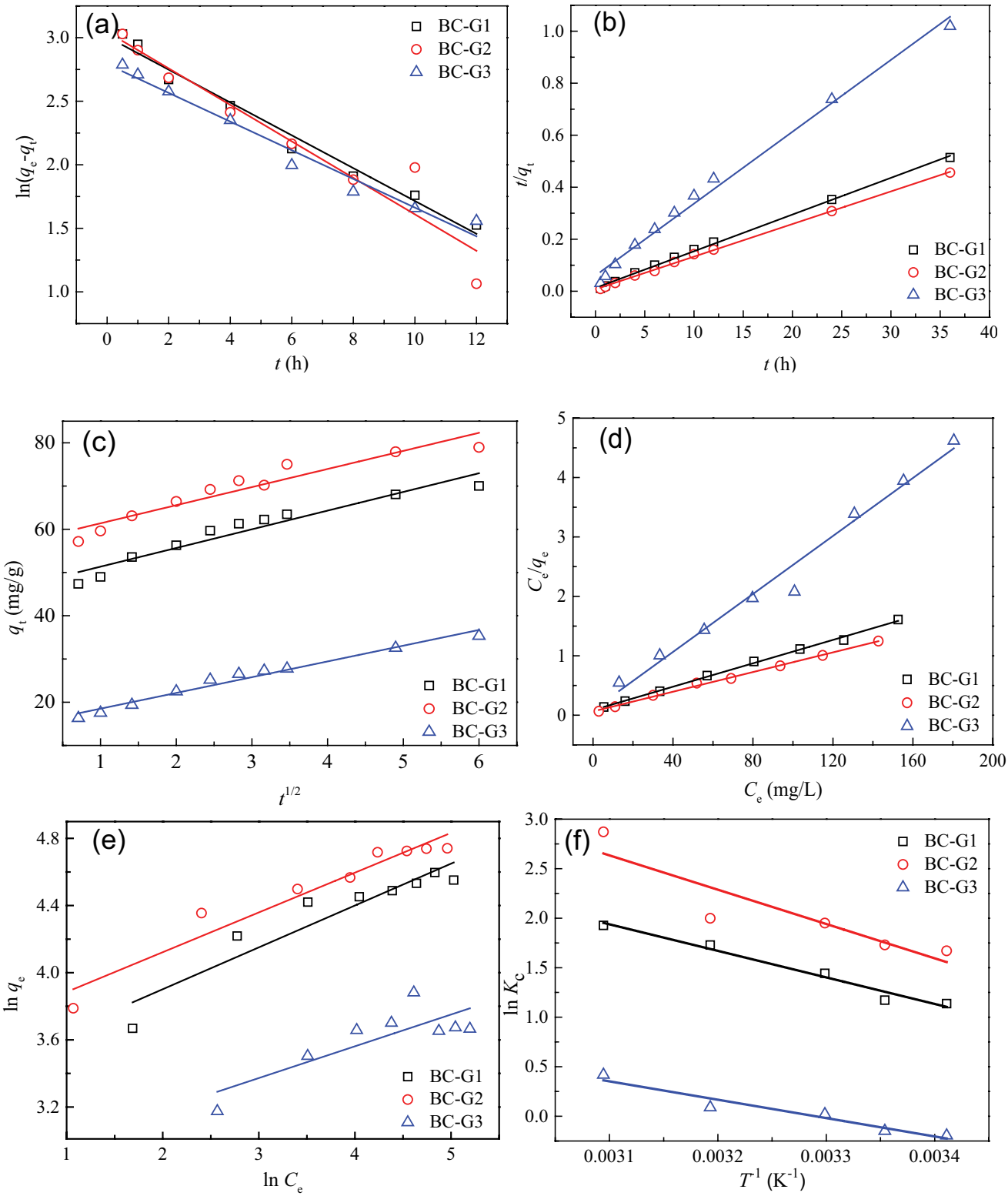

Fig. 7. The pseudo-first-order model (a), the pseudo-second-order model (b), the intraparticle diffusion model (c), Langmuir model (d), Freundlich model (e) and Van't Hoff plot (f) of Cr(VI) adsorption on BC-G1, BC-G2 and BC-G3.

Table 5
Thermodynamic parameters for Cr(VI) adsorption by BC-G1, BC-G2 and BC-G3

Sorbents	$\Delta H°$ (kJ/mol)	$\Delta S°$ (J/mol/K)	$\Delta G°$ (kJ/mol)				
			20°C (293 K)	25°C (298 K)	30°C (303 K)	40°C (313 K)	50°C (323 K)
BC-G1	28.8062	111.2002	–3.7755	–4.3315	–4.8875	–5.9995	–7.1115
BC-G2	22.2917	85.2187	–2.6774	–3.1035	–3.5296	–4.3818	–5.2339
BC-G3	15.4241	50.7444	0.5560	0.3023	0.0486	–0.4589	–0.9663

Table 6
Summary of the maximum adsorption capacities of various modified biochar to Cr(VI) in the literature

Adsorbents	Adsorption capacity (mg/g)	Temperature (°C)	pH	References
Iron-modified corn straw biochar	97.43	25	7	[3]
$FeCl_3$ and $ZnCl_2$-modified corn stalks biochar	138.89	30 ± 1	2	[4]
Mg/Al-layered double hydroxide intercalated with ethylenediaminetetraacetic acid modified bamboo shavings biochar	52.22	27 ± 0.5	3	[7]
Urea modified poplar leaf biochar	28.3	25	3	[13]
Fe_3O_4@SiO_2-NH_2 particles modified phoenix tree leaves biochar	27.2	30	1	[28]
Nano ZnO/ZnS modified corn stover biochar	24.5	25 ± 0.5	No pH adjustment	[61]
Cationic surfactant modified *Auricularia auricula* dreg biochar	24.9	25	2	[62]
Polyamidoamine dendrimer modified rice straw biochar	101.52 120.77 40.98	30	2	This study

284.7, 285.8, and 287.7 eV were assigned to C–C, C–N, and C=O bonding, respectively [25,55]. After binding to Cr(VI), the change in the binding energy of C–C was almost insignificant, but that of C–N and C=O increased to 285.9 and 288.1 eV, respectively. This phenomenon may be attributed to the interaction between neighboring N and metal ions [25]. In addition, the high-resolution N 1s spectra of BC-G2 before adsorption of Cr(VI) (Fig. 8e) showed that the two peaks appeared at binding energies of 399.6 and 401.5 eV, which were attributed to amines $–NH_2$ and amide bonds N–C=O, respectively [44]. These specific peaks shift to higher binding energies (399.7 and 401.6 eV, respectively), as shown in Fig. 8f, after the adsorption of Cr(VI), indicating the participation of $–NH_2$ groups and amide bonds N–C=O in the Cr(VI) adsorption process, which led to the decrease in electron density and the increase in the binding energy of nitrogen and oxygen atoms [46]. In acidic pH, $–NH_2$ protonation contributed to the electrostatic interaction with $HCrO4^-$ [29], which led to Cr(VI) reduction, resulting in Cr(III) formation between N–C=O and Cr(VI) [56]. Then, a chelated complex was formed by coordination between the newly formed Cr(III) and $–NH_2$ group due to the empty orbital and the lone pair of electrons of Cr(III) cation and the amine group, respectively [1].

Meanwhile, the weak attractive interactions between BC-G2 and $HCrO_4^-$ (BC-G2-$HCrO_4^-$) or $Cr_2O_7^{2-}$ (BC-G2-$Cr_2O_7^{2-}$) were studied using an independent gradient model (IGM) analysis, described by Lefebvre et al. [57]. The IGM interactions were studied using Multiwfn software [58]. The visualization of IGM and orbitals was rendered by VMD [59]. The results are shown in Fig. 9; blue colors represent the strong attractions, and green colors denote the van der Waals force. The presence of N–H···O and C–H···O hydrogen bonding interactions and van der Waals force in the BC-G2-$HCrO_4^-$ (Fig. 9a) and BC-G2-$Cr_2O_7^{2-}$ (Fig. 9b) system are thus evident [60].

Based on the above analysis, the adsorption of Cr(VI) using BC-G2 was as follows: (1) Cr(VI) was adsorbed on the surface of BC-G2 through the electrostatic interaction between the negatively charged Cr(VI) species and the protonated amine groups; (2) with the assistance of electron donors (the amino groups), Cr(VI) was reduced to Cr(III); and (3) part of Cr(III) coordinated with the $–NH_2$ group to form a chelated complex through the shared bond between N and Cr(III); at the same time, Cr(III) was also released into solution under the electrostatic repulsion between the Cr(III) and the protonated amine groups [1,25,54]. Furthermore, hydrogen bonding and van der Waals force also contributed to the adsorption process.

3.5. Regeneration properties

Regeneration and recycling of adsorbents are important factors in reducing the cost of the adsorption process

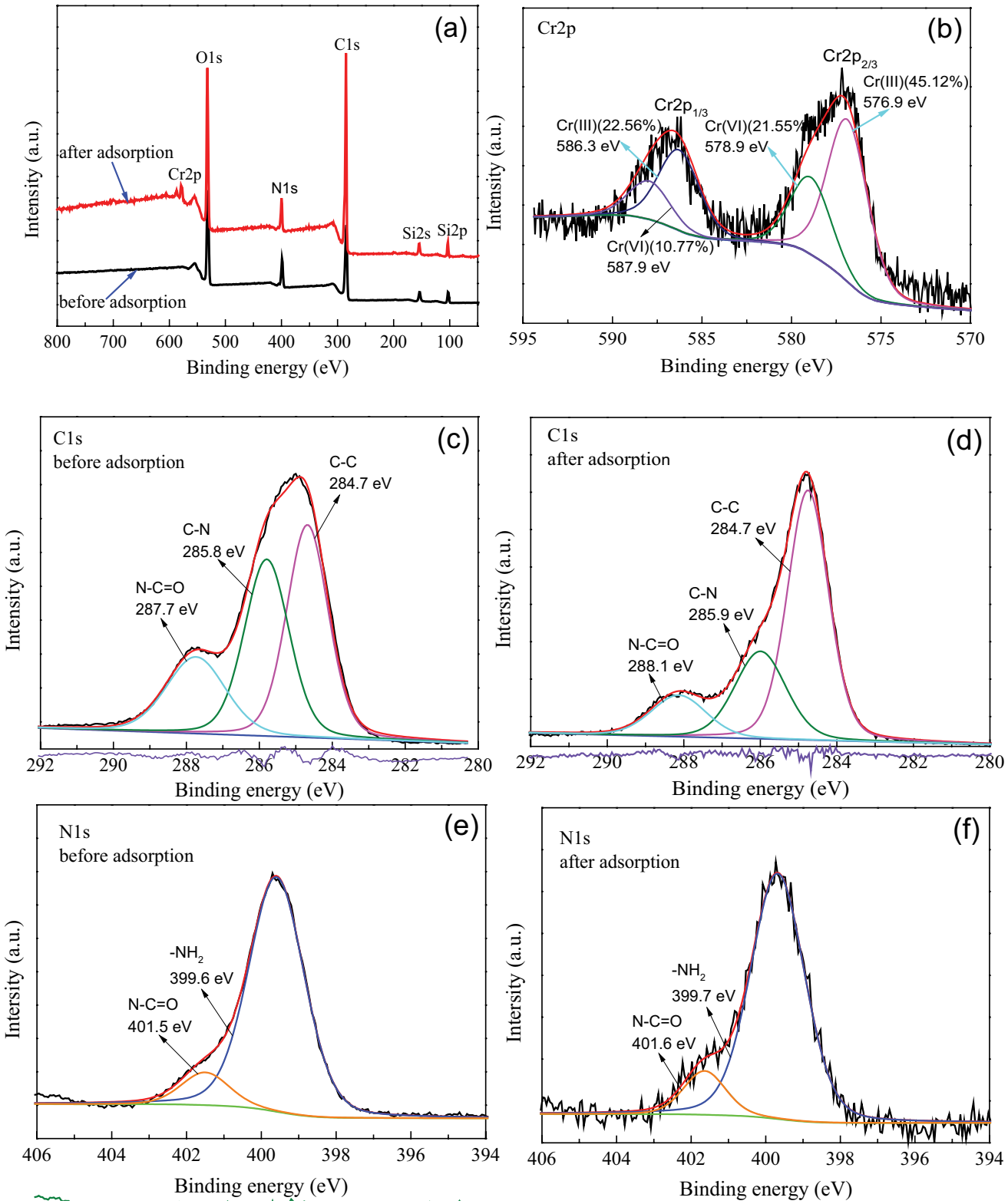

Fig. 8. XPS spectra of survey scan of BC-G2 before and after adsorption of Cr(VI) (a), high-resolution scan of Cr 2p (b), C 1s (c, d) and N 1s (e, f) of BC-G2 before and after adsorption of Cr(VI).

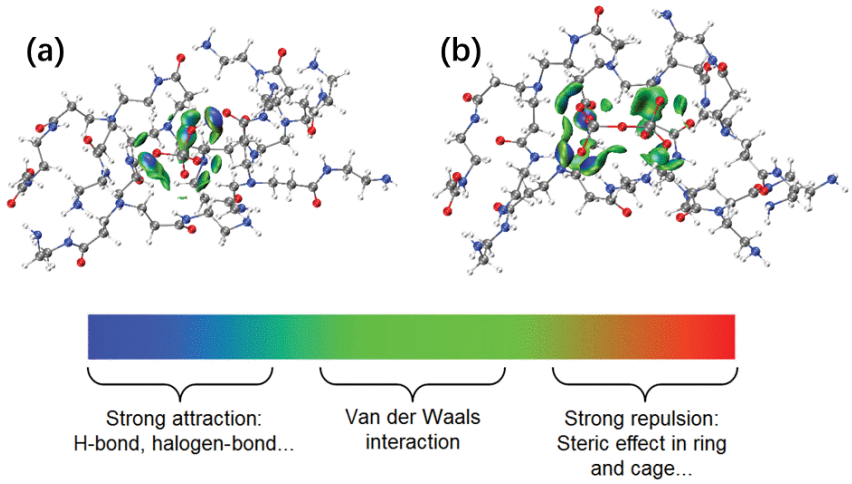

Fig. 9. Visual weak interactions of BC-G2-$HCrO_4^-$ (a) and BC-G2-$Cr_2O_7^{2-}$ (b) described by the IGM method (Cr-purple, H-white, O-red, C-gray, N-blue).

in practical applications. Since higher pH (as mentioned earlier) resulted in the low adsorption of Cr(VI), the desorption experiments were conducted in a 0.2 M NaOH solution. As shown in Fig. 10, the adsorption capacity of BC-G1 decreased to 45.13 mg/g after the third desorption treatment. However, the adsorption capacity of BC-G2 could still reach 61.29 mg/g for the fourth adsorption–desorption cycle, indicating that the decrease in the adsorption capacity was insignificant compared to that of the first cycle. The results suggested that the BC-G2 adsorbent was reliable and can be reused several times in future practical applications.

3.6. Comparison of the maximum adsorption capacity

Table 6 summarizes the maximum adsorption capacities of various modified biochars for Cr(VI) in the literature. The Langmuir maximum adsorption capacity of BC-G1, BC-G2, and BC-G3 for Cr(VI) was 101.52, 120.77, and 40.98 mg/g, respectively, which was significantly higher than that of many adsorbents, thus suggesting that the PAMAM-modified biochar adsorbents might be potential adsorbents for removing Cr(VI) from wastewater.

4. Conclusions

In this study, three novel and cost-effective PAMAM dendrimer-modified biochar adsorbents were successfully prepared for removing Cr(VI) from aqueous media. The introduction of amino functional groups to the fabricated adsorbents greatly improved their adsorption performance compared to the raw biochar from the experimental data. The adsorption capacity of modified biochar adsorbents was enhanced with increasing generation number of PAMAM dendrimer, while the strong steric hindrance led to a lower percentage of functional groups on the basal plane of BC-G3, decreasing the adsorption capacity of BC-G3. The maximum Cr(VI) adsorption capacity of BC-G1, BC-G2, and BC-G3 was 101.52, 120.77, and 40.98 mg/g at 30°C, respectively. The adsorption data of all the biochar adsorbents were in good agreement with the pseudo-second-order model and

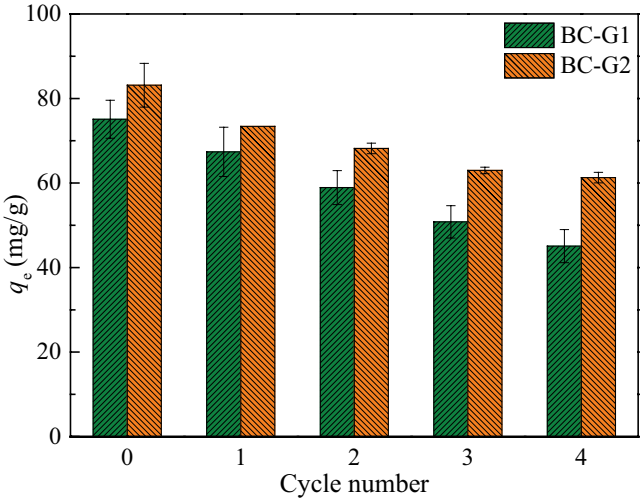

Fig. 10. Adsorption and desorption cycles performance of BC-G1 and BC-G2 for Cr(VI).

followed the Langmuir adsorption with monolayer coverage. Thermodynamics studies showed that the Cr(VI) adsorption onto BC-G1 and BC-G2 was a spontaneous endothermic process, while BC-G3 showed non-spontaneous behavior when the temperature was below 30°C. The possible removal mechanism of BC-G2 was proposed, which involves the electrostatic interaction, surface complexation, and reduction for Cr(VI) removal. The regeneration property test suggested that the decrease in the adsorption capacity of BC-G2 was insignificant for four adsorption–desorption cycles. Thus, PAMAM dendrimer-modified biochar adsorbent BC-G2 would be a potential cost-effective adsorbent for removing Cr(VI) from wastewater.

Acknowledgements

This work was supported by the National Key Research and Development Project of China (2018YFC1802603), the National Natural Science Foundation of China (52060011),

the Basic Research Programs of Yunnan Province (202101AU070038, 202101AT070129 and 202101BE070001-024), the Analysis and Testing Foundation of Kunming University of Science and Technology (2020P20191107004) and Key Laboratory of Water Pollution Treatment and Resource Reuse of Hainan Province. The authors also wish to thanks to the anonymous reviewers and editor for their helpful suggestions and enlightening comments to improve the manuscript quality.

References

[1] Y. Tadjenant, N. Dokhan, A. Barras, A. Addad, R. Jijie, S. Szunerits, R. Boukherroub, Graphene oxide chemically reduced and functionalized with KOH-PEI for efficient Cr(VI) adsorption and reduction in acidic medium, Chemosphere, 258 (2020) 127316, doi: 10.1016/j.chemosphere.2020.127316.

[2] X. Wang, J. Xu, J. Liu, J. Liu, F. Xia, C. Wang, R.A. Dahlgren, W. Liu, Mechanism of Cr(VI) removal by magnetic greigite/biochar composites, Sci. Total Environ., 700 (2020) 134414, doi: 10.1016/j.scitotenv.2019.134414.

[3] J. Wen, Z. Xue, X. Yin, X. Wang, Insights into aqueous reduction of Cr(VI) by biochar and its iron-modified counterpart in the presence of organic acids, Chemosphere, 286 (2022) 131918, doi: 10.1016/j.chemosphere.2021.131918.

[4] Y. Yu, Q. An, L. Jin, N. Luo, Z. Li, J. Jiang, Unraveling sorption of Cr(VI) from aqueous solution by $FeCl_3$ and $ZnCl_2$-modified corn stalks biochar: implicit mechanism and application, Bioresour. Technol., 297 (2020) 122466, doi: 10.1016/j.biortech.2019.122466.

[5] A.V. Borhade, B.K. Uphade, Removal of chromium(VI) from aqueous solution using modified CdO nanoparticles, Desal. Water Treat., 57 (2015) 9776–9788.

[6] M.M. Kabir, M.M. Akter, S. Khandaker, B.H. Gilroyed, M. Didar-ul-Alam, M. Hakim, M.R. Awual, Highly effective agro-waste based functional green adsorbents for toxic chromium(VI) ion removal from wastewater, J. Mol. Liq., 347 (2022) 118327, doi: 10.1016/j.molliq.2021.118327.

[7] D. Huang, C. Liu, C. Zhang, R. Deng, R. Wang, W. Xue, H. Luo, G. Zeng, Q. Zhang, X. Guo, Cr(VI) removal from aqueous solution using biochar modified with Mg/Al-layered double hydroxide intercalated with ethylenediaminetetraacetic acid, Bioresour. Technol., 276 (2019) 127–132.

[8] F.-X. Dong, L. Yan, X.-H. Zhou, S.-T. Huang, J.-Y. Liang, W.-X. Zhang, Z.-W. Guo, P.-R. Guo, W. Qian, L.-J. Kong, W. Chu, Z.-H. Diao, Simultaneous adsorption of Cr(VI) and phenol by biochar-based iron oxide composites in water: performance, kinetics and mechanism, J. Hazard. Mater., 416 (2021) 125930, doi: 10.1016/j.jhazmat.2021.125930.

[9] M.R. Awual, Assessing of lead(III) capturing from contaminated wastewater using ligand doped conjugate adsorbent, Chem. Eng. J., 289 (2016) 65–73.

[10] M.R. Awual, A facile composite material for enhanced cadmium(II) ion capturing from wastewater, J. Environ. Chem. Eng., 7 (2019) 103378, doi: 10.1016/j.jece.2019.103378.

[11] L. Liu, X. Liu, D. Wang, H. Lin, L. Huang, Removal and reduction of Cr(VI) in simulated wastewater using magnetic biochar prepared by co-pyrolysis of nano-zero-valent iron and sewage sludge, J. Cleaner Prod., 257 (2020) 120562, doi: 10.1016/j.jclepro.2020.120562.

[12] K.T. Kubra, M.S. Salman, M.N. Hasan, A. Islam, M.M. Hasan, M.R. Awual, Utilizing an alternative composite material for effective copper(II) ion capturing from wastewater, J. Mol. Liq., 336 (2021) 116325, doi: 10.1016/j.molliq.2021.116325.

[13] N. Zhao, C. Zhao, D.C.W. Tsang, K. Liu, L. Zhu, W. Zhang, J. Zhang, Y. Tang, R. Qiu, Microscopic mechanism about the selective adsorption of Cr(VI) from salt solution on O-rich and N-rich biochars, J. Hazard. Mater., 404 (2021) 124162, doi: 10.1016/j.jhazmat.2020.124162.

[14] K. Komnitsas, D. Zaharaki, G. Bartzas, G. Kaliakatsou, A. Kritikaki, Efficiency of pecan shells and sawdust biochar on Pb and Cu adsorption, Desal. Water Treat., 57 (2016) 3237–3246.

[15] J. Liu, W. Cheng, X. Yang, Y. Bao, Modification of biochar with silicon by one-step sintering and understanding of adsorption mechanism on copper ions, Sci. Total Environ., 704 (2020) 135252, doi: 10.1016/j.scitotenv.2019.135252.

[16] Y. Ma, W.-J. Liu, N. Zhang, Y.-S. Li, H. Jiang, G.-P. Sheng, Polyethylenimine modified biochar adsorbent for hexavalent chromium removal from the aqueous solution, Bioresour. Technol., 169 (2014) 403–408.

[17] C. Jeon, K.L. Solis, H.-R. An, Y. Hong, A.D. Igalavithana, Y.S. Ok, Sustainable removal of Hg(II) by sulfur-modified pine-needle biochar, J. Hazard. Mater., 388 (2020) 122048, doi: 10.1016/j.jhazmat.2020.122048.

[18] H. Li, X. Dong, E.B. da Silva, L.M. de Oliveira, Y. Chen, L.Q. Ma, Mechanisms of metal sorption by biochars: biochar characteristics and modifications, Chemosphere, 178 (2017) 466–478.

[19] A. Ekanayake, A.U. Rajapaksha, R. Selvasembian, M. Vithanage, Amino-functionalized biochars for the detoxification and removal of hexavalent chromium in aqueous media, Environ. Res., 211 (2022) 113073.

[20] Y.-R. Lee, S. Zhang, K. Yu, J. Choi, W.-S. Ahn, Poly(amidoamine) dendrimer immobilized on mesoporous silica foam (MSF) and fibrous nano-silica KCC-1 for Gd^{3+} adsorption in water, Chem. Eng. J., 378 (2019) 122133, doi: 10.1016/j.cej.2019.122133.

[21] J. Zhao, X. Zhang, X. He, M. Xiao, W. Zhang, C. Lu, A super biosorbent from dendrimer poly(amidoamine)-grafted cellulose nanofibril aerogels for effective removal of Cr(VI), J. Mater. Chem. A, 3 (2015) 14703–14711.

[22] Y. Zhou, L. Luan, B. Tang, Y. Niu, R. Qu, Y. Liu, W. Xu, Fabrication of Schiff base decorated PAMAM dendrimer/magnetic Fe_3O_4 for selective removal of aqueous Hg(II), Chem. Eng. J., 398 (2020) 125651, doi: 10.1016/j.cej.2020.125651.

[23] B. Hayati, A. Maleki, F. Najafi, H. Daraei, F. Gharibi, G. Mckay, Super high removal capacities of heavy metals (Pb^{2+} and Cu^{2+}) using CNT dendrimer, J. Hazard. Mater., 336 (2017) 146–157.

[24] L. Zhou, Y. Duan, X. Xu, Facile preparation of amine-rich polyamidoamine (PAMAM) gel for highly efficient removal of Cr(VI) ions, Colloids Surf., A, 579 (2019) 123685, doi: 10.1016/j.colsurfa.2019.123685.

[25] H. Liu, F. Zhang, Z. Peng, Adsorption mechanism of Cr(VI) onto GO/PAMAMs composites, Sci. Rep., 9 (2019) 3663, doi: 10.1038/s41598-019-40344-9.

[26] K. Sarkar, P.P. Kundu, Preparation of low molecular weight N-maleated chitosan-*graft*-PAMAM copolymer for enhanced DNA complexation, Int. J. Biol. Macromol., 51 (2012) 859–867.

[27] X. Zhang, L. Lv, Y. Qin, M. Xu, X. Jia, Z. Chen, Removal of aqueous Cr(VI) by a magnetic biochar derived from melia azedarach wood, Bioresour. Technol., 256 (2018) 1–10.

[28] S. Shi, J. Yang, S. Liang, M. Li, Q. Gan, K. Xiao, J. Hu, Enhanced Cr(VI) removal from acidic solutions using biochar modified by Fe_3O_4@SiO_2-NH_2 particles, Sci. Total Environ., 628 (2018) 499–508.

[29] M.M. Mian, G. Liu, B. Yousaf, B. Fu, H. Ullah, M.U. Ali, Q. Abbas, M.A.M. Munir, L. Ruijia, Simultaneous functionalization and magnetization of biochar via NH_3 ambiance pyrolysis for efficient removal of Cr(VI), Chemosphere, 208 (2018) 712–721.

[30] M.R. Awual, T. Yaita, H. Shiwaku, S. Suzuki, A sensitive ligand embedded nano-conjugate adsorbent for effective cobalt(II) ions capturing from contaminated water, Chem. Eng. J., 276 (2015) 1–10.

[31] J. Qu, Y. Yuan, Q. Meng, G. Zhang, F. Deng, L. Wang, Y. Tao, Z. Jiang, Y. Zhang, Simultaneously enhanced removal and stepwise recovery of atrazine and Pb(II) from water using β–cyclodextrin functionalized cellulose: characterization, adsorptive performance and mechanism exploration, J. Hazard. Mater., 400 (2020) 123142, doi: 10.1016/j.jhazmat.2020.123142.

[32] J. Dai, X. Meng, Y. Zhang, Y. Huang, Effects of modification and magnetization of rice straw derived biochar on adsorption of tetracycline from water, Bioresour. Technol., 311 (2020) 123455, doi: 10.1016/j.biortech.2020.123455.

[33] Z. Shen, D. Hou, F. Jin, J. Shi, X. Fan, D.C.W. Tsang, D.S. Alessi, Effect of production temperature on lead removal mechanisms by rice straw biochars, Sci. Total Environ., 655 (2019) 751–758.
[34] M.N. Hasan, M.A. Shenashen, M.M. Hasan, H. Znad, M.R. Awual, Assessing of cesium removal from wastewater using functionalized wood cellulosic adsorbent, Chemosphere, 270 (2021) 128668, doi: 10.1016/j.chemosphere.2020.128668.
[35] J.L. Vidal, V.P. Andrea, S.L. MacQuarrie, F.M. Kerton, Oxidized biochar as a simple, renewable catalyst for the production of cyclic carbonates from carbon dioxide and epoxides, ChemCatChem, 11 (2019) 4089–4095.
[36] B. Hayati, A. Maleki, F. Najafi, F. Gharbi, G. Mckay, V.K. Gupta, S.H. Puttaiah, N. Marzban, Heavy metal adsorption using PAMAM/CNT nanocomposite from aqueous solution in batch and continuous fixed bed systems, Chem. Eng. J., 346 (2018) 258–270.
[37] W. Qin, G. Qian, H. Tao, J. Wang, J. Sun, X. Cui, Y. Zhang, X. Zhang, Adsorption of Hg(II) ions by PAMAM dendrimers modified attapulgite composites, React. Funct. Polym., 136 (2019) 75–85.
[38] L. Qian, S. Liu, W. Zhang, Y. Chen, D. Ouyang, L. Han, J. Yan, M. Chen, Enhanced reduction and adsorption of hexavalent chromium by palladium and silicon rich biochar supported nanoscale zero-valent iron, J. Colloid Interface Sci., 533 (2019) 428–436.
[39] W. Yu, J. Hu, Y. Yu, D. Ma, W. Gong, H. Qiu, Z. Hu, H.-W. Gao, Facile preparation of sulfonated biochar for highly efficient removal of toxic Pb(II) and Cd(II) from wastewater, Sci. Total Environ., 750 (2021) 141545, doi: 10.1016/j.scitotenv.2020.141545.
[40] M.R. Awual, Solid phase sensitive palladium(II) ions detection and recovery using ligand based efficient conjugate nanomaterials, Chem. Eng. J., 300 (2016) 264–272.
[41] M.R. Awual, T. Yaita, S. Suzuki, H. Shiwaku, Ultimate selenium(IV) monitoring and removal from water using a new class of organic ligand based composite adsorbent, J. Hazard. Mater., 291 (2015) 111–119.
[42] M.R. Awual, Efficient phosphate removal from water for controlling eutrophication using novel composite adsorbent, J. Cleaner Prod., 228 (2019) 1311–1319.
[43] X. Zhou, J. Zhou, Y. Liu, J. Guo, J. Ren, F. Zhou, Preparation of iminodiacetic acid-modified magnetic biochar by carbonization, magnetization and functional modification for Cd(II) removal in water, Fuel, 233 (2018) 469–479.
[44] Y.-X. Ma, D. Xing, W.-J. Shao, X.-Y. Du, P.-Q. La, Preparation of polyamidoamine dendrimers functionalized magnetic graphene oxide for the adsorption of Hg(II) in aqueous solution, J. Colloid Interface Sci., 505 (2017) 352–363.
[45] Z. Mahdi, A.E. Hanandeh, Q.J. Yu, Preparation, characterization and application of surface modified biochar from date seed for improved lead, copper, and nickel removal from aqueous solutions, J. Environ. Chem. Eng., 7 (2019) 103379, doi: 10.1016/j.jece.2019.103379.
[46] X. Zhou, Y. Liu, J. Zhou, J. Guo, J. Ren, F. Zhou, Efficient removal of lead from aqueous solution by urea-functionalized magnetic biochar: preparation, characterization and mechanism study, J. Taiwan Inst. Chem. Eng., 91 (2018) 457–467.
[47] M.R. Awual, T. Yaita, T. Kobayashi, H. Shiwaku, S. Suzuki, Improving cesium removal to clean-up the contaminated water using modified conjugate material, J. Environ. Chem. Eng., 8 (2020) 103684, doi: 10.1016/j.jece.2020.103684.
[48] H. Ma, J. Yang, X. Gao, Z. Liu, X. Liu, Z. Xu, Removal of chromium(VI) from water by porous carbon derived from corn straw: influencing factors, regeneration and mechanism, J. Hazard. Mater., 369 (2019) 550–560.
[49] N. Liu, Y. Zhang, C. Xu, P. Liu, J. Lv, Y.Y. Liu, Q. Wang, Removal mechanisms of aqueous Cr(VI) using apple wood biochar: a spectroscopic study, J. Hazard. Mater., 384 (2020) 121371, doi: 10.1016/j.jhazmat.2019.121371.
[50] Y. Zhang, M. Li, J. Li, Y. Yang, X. Liu, Surface modified leaves with high efficiency for the removal of aqueous Cr(VI), Appl. Surf. Sci., 484 (2019) 189–196.
[51] H. Zhang, R. Xiao, R. Li, A. Ali, A. Chen, Z. Zhang, Enhanced aqueous Cr(VI) removal using chitosan-modified magnetic biochars derived from bamboo residues, Chemosphere, 261 (2020) 127694, doi: 10.1016/j.chemosphere.2020.127694.
[52] M.R. Awual, A novel facial composite adsorbent for enhanced copper(II) detection and removal from wastewater, Chem. Eng. J., 266 (2015) 368–375.
[53] M.R. Awual, Ring size dependent crown ether based mesoporous adsorbent for high cesium adsorption from wastewater, Chem. Eng. J., 303 (2016) 539–546.
[54] Q. Kong, J. Wei, Y. Hu, C. Wei, Fabrication of terminal amino hyperbranched polymer modified graphene oxide and its prominent adsorption performance towards Cr(VI), J. Hazard. Mater., 363 (2019) 161–169.
[55] Y.-X. Ma, Y.-L. Kou, D. Xing, P.-S. Jin, W.-J. Shao, X. Li, X.-Y. Du, P.-Q. La, Synthesis of magnetic graphene oxide grafted polymaleicamide dendrimer nanohybrids for adsorption of Pb(II) in aqueous solution, J. Hazard. Mater., 340 (2017) 407–416.
[56] W. Cai, J. Wei, Z. Li, Y. Liu, J. Zhou, B. Han, Preparation of amino-functionalized magnetic biochar with excellent adsorption performance for Cr(VI) by a mild one-step hydrothermal method from peanut hull, Colloids Surf., A, 563 (2019) 102–111.
[57] C. Lefebvre, G. Rubez, H. Khartabil, J.-C. Boisson, J. Contreras-García, E. Hénon, Accurately extracting the signature of intermolecular interactions present in the NCI plot of the reduced density gradient versus electron density, Phys. Chem. Chem. Phys., 19 (2017) 17928–17936.
[58] T. Lu, F. Chen, Multiwfn: a multifunctional wavefunction analyzer, J. Comput. Chem., 33 (2012) 580–592.
[59] W. Humphrey, A. Dalke, K. Schulten, VMD: visual molecular dynamics, J. Mol. Graphics, 14 (1996) 33–38.
[60] Q.-Y. Yang, Y.-M. Zhang, X.-Q. Ma, H.-Q. Dong, Y.-F. Zhang, W.-L. Guan, H. Yao, T.-B. Wei, Q. Lin, A pillar[5]arene-based fluorescent sensor for sensitive detection of L-Met through a dual-site collaborative mechanism, Spectrochim. Acta, Part A, 240 (2020) 118569, doi: 10.1016/j.saa.2020.118569.
[61] C. Li, L. Zhang, Y. Gao, A. Li, Facile synthesis of nano ZnO/ZnS modified biochar by directly pyrolyzing of zinc contaminated corn stover for Pb(II), Cu(II) and Cr(VI) removals, Waste Manage., 79 (2018) 625–637.
[62] Y. Li, Y. Wei, S. Huang, X. Liu, Z. Jin, M. Zhang, J. Qu, Y. Jin, Biosorption of Cr(VI) onto *Auricularia auricula* dreg biochar modified by cationic surfactant: characteristics and mechanism, J. Mol. Liq., 269 (2018) 824–832.